Synthesis of a Novel Porous Polymer/Ceramic Composite Material by Low-Temperature Atomic Layer Deposition

Xinhua Liang, Steven M. George, and Alan W. Weimer*

Department of Chemical and Biological Engineering, University of Colorado, Boulder, Colorado 80309

Nai-Hong Li

Polygenetics Incorporated, Mountain View, California 94043

John H. Blackson and Joseph D. Harris

Dow Chemical Company, Midland, Michigan 48667

Peng Li

Department of Earth and Planetary Sciences, University of New Mexico, Albuquerque, New Mexico 87131

Received May 25, 2007. Revised Manuscript Received August 10, 2007

Highly porous poly(styrene-divinylbenzene) particles (∼85% porosity, 8−10 cm^3/g pore volume, 43.5 m^2/g surface area, 70 kg/m^3 particle density, and ∼600 μm diameter) were synthesized by copolymerization of styrene and divinylbenzene. Conformal alumina films were grown on internal and external polymer particle surfaces at 33 °C by atomic layer deposition (ALD). Analytical characterization revealed that the pore filling mechanism was a uniform coating of the pore walls. ALD provides a controllable method for reinforcing porous polymeric structures while modifying surface properties. Such surface functionalization may promote cell adhesion and proliferation for tissue engineering applications.

Introduction

Porous polymers have gained increased interest in the field of tissue engineering.[1−7] This is attributed to their unique physicochemical properties, such as an interconnected pore structure, large surface area, and small pore size. Ideally, tissue engineering materials should be designed to be biocompatible and bioactive so that they can receive and respond to specific biological signals, which direct and promote cell adhesion, proliferation, differentiation, and tissue regeneration.[7−9] However, the porous structure of neat polymers adversely impacts the mechanical properties and biocompatibility of porous polymers. Ceramics, such as alumina and titania, have an excellent biocompatibility and bone bonding.[10−12] A novel process to produce reinforced porous structures with an enhanced biocompatibility and improved tissue interaction is to coat the inside of the pores as well as the surface of the porous polymers with ultrathin ceramic films while maintaining the original structure and properties of the substrates.

In many practical applications, porous polymer/ceramic composites are often produced via incipient wetting methods.[9,12−15] The solvent-based methods have the risk of

* Corresponding author. E-mail: alan.weimer@colorado.edu.

(1) Wang, X. X.; Li, W.; Kumar, V. A method for solvent-free fabrication of porous polymer using solid-state foaming and ultrasound for tissue engineering applications. *Biomaterials* **2006**, *27* (9), 1924−1929.
(2) Northen, T. R.; Brune, D. C.; Woodbury, N. W. Synthesis and characterization of peptide grafted porous polymer microstructures. *Biomacromolecules* **2006**, *7* (3), 750−754.
(3) Bokhari, M. A.; Akay, G.; Zhang, S. G.; Birch, M. A. The enhancement of osteoblast growth and differentiation in vitro on a peptide hydrogel−polyHIPE polymer hybrid material. *Biomaterials* **2005**, *26* (25), 5198−5208.
(4) Macintyre, F. S.; Sherrington, D. C.; Tetley, L. Synthesis of ultrahigh surface area monodisperse porous polymer nanospheres. *Macromolecules* **2006**, *39* (16), 5381−5384.
(5) Menner, A.; Haibach, K.; Powell, R.; Bismarck, A. Tough reinforced open porous polymer foams via concentrated emulsion templating. *Polymer* **2006**, *47* (22), 7628−7635.
(6) Tienen, T. G.; Heijkants, R. G. J. C.; de Groot, J. H.; Pennings, A. J.; Schouten, A. J.; Veth, R. P. H.; Buma, P. Replacement of the knee meniscus by a porous polymer implant−A study in dogs. *Am. J. Sports Med.* **2006**, *34* (1), 64−71.
(7) Ma, P. X.; Zhang, R. Y.; Xiao, G. Z.; Franceschi, R. Engineering new bone tissue in vitro on highly porous poly(α-hydroxyl acids)/hydroxyapatite composite scaffolds. *J. Biomed. Mater. Res.* **2001**, *54* (2), 284−293.
(8) Chapekar, M. S. Tissue engineering: Challenges and opportunities. *J. Biomed. Mater. Res.* **2000**, *53* (6), 617−620.
(9) Liu, X. H.; Won, Y. J.; Ma, P. X. Surface modification of interconnected porous scaffolds. *J. Biomed. Mater. Res., Part A* **2005**, *74* (1), 84−91.
(10) Warashina, H.; Sakano, S.; Kitamura, S.; Yamauchi, K. I.; Yamaguchi, J.; Ishiguro, N.; Hasegawa, Y. Biological reaction to alumina, zirconia, titanium, and polyethylene particles implanted onto murine calvaria. *Biomaterials* **2003**, *24* (21), 3655−3661.
(11) Takami, Y.; Nakazawa, T.; Makinouchi, K.; Glueck, J.; Nose, Y. Biocompatibility of alumina ceramic and polyethylene as materials for pivot bearings of a centrifugal blood pump. *J. Biomed. Mater. Res.* **1997**, *36* (3), 381−386.
(12) Rezwan, K.; Chen, Q. Z.; Blaker, J. J.; Boccaccini, A. R. Biodegradable and bioactive porous polymer/inorganic composite scaffolds for bone tissue engineering. *Biomaterials* **2006**, *27* (18), 3413−3431.
(13) Kim, J. W.; Lee, J. E.; Kim, S. J.; Lee, J. S.; Ryu, J. H.; Kim, J.; Han, S. H.; Chang, I. S.; Suh, K. D. Synthesis of silver/polymer colloidal composites from surface-functional porous polymer microspheres. *Polymer* **2004**, *45* (14), 4741−4747.
(14) Rifai, S.; Breen, C. A.; Solis, D. J.; Swager, T. M. Facile in situ silver nanoparticle formation in insulating porous polymer matrices. *Chem. Mater.* **2006**, *18* (1), 21−25.

10.1021/cm071431k CCC: $37.00
Published on Web 09/26/2007

leaving potentially toxic organic solvent residues. Depositing ultrathin films inside the pores as well as on the surface of the porous polymers by methods such as chemical vapor deposition (CVD) is difficult to impossible. Typical CVD processes require high operating temperatures,[16−18] which are much higher than the softening and melting temperatures of the polymers. During CVD reactions, the chemical reactants are allowed to coexist in the gas phase, so CVD methods are not able to effectively control the use of precursor gases or to inherently control the location and thickness of the ceramic films. Films grown by CVD will block the pores of the porous polymers.

Atomic layer deposition (ALD) is a surface controlled layer-by-layer process[19−22] that is particularly well-suited for depositing ultrathin and conformal films onto porous substrates. The films grown by ALD are inherently controlled by self-limiting sequential surface chemical reactions, so precursors are used efficiently. The advantages of ALD methods include low impurity content, pinhole-free deposition, low processing temperature, and independence of line of sight.[19−22] As a result, ultrathin films can be uniformly formed inside the pores as well as on the surface of the porous substrates.

Alumina is biocompatible,[11] and alumina films have been deposited on several substrates by ALD.[21−30] Alumina ALD is carried out according to the following two surface reactions:

$$\mathrm{AlOH^* + Al(CH_3)_3 \rightarrow [AlOAl(CH_3)_2]^* + CH_4} \quad (1)$$

$$\mathrm{Al(CH_3)^* + H_2O \rightarrow AlOH^* + CH_4} \quad (2)$$

where the asterisks denote the surface species.[20−22] Each reaction is self-limiting, and the completion of each reaction provides the necessary chemical functional groups to facilitate the subsequent reaction. When performed in an ABAB reaction sequence, these sequential reactions produce linear, atomic layer controlled alumina films.

The main objective of this research was to fabricate a novel porous polymer/ceramic composite material for tissue engineering applications. In the present study, high internal phase emulsion (HIPE)-based highly porous poly(styrene-divinylbenzene) (PS−DVB) particles were synthesized by the copolymerization of styrene and divinylbenzene. Ultrathin alumina films were successfully deposited in the pores of highly porous PS−DVB particles by ALD in a scalable fluidized bed reactor at 33 °C.

Experimental Procedures

Synthesis of Porous PS−DVB Particles.[31,32] A HIPE was formed by combining precursor oil and aqueous discontinuous phases while subjecting the combination to shear agitation. Once formed, the HIPE was added to the aqueous suspension medium. The HIPE must be added to the suspension medium in an amount and at a rate suitable for forming a suspension of HIPE microdroplets. As the HIPE was added, the suspension was subjected to sufficient shear agitation to form a stable suspension. Once a stable suspension of HIPE microdroplets was obtained, the temperature of the aqueous suspension medium was increased above ambient temperature, and polymerization was initiated. The polymerization step converted a HIPE microdroplet to a solid particle. This particle was generally washed to remove any residual unpolymerized components of the HIPE or the suspension medium.

For a typical run, an oil phase was prepared by combining 11.37 g of styrene-based monomer, 11.25 g of DVB, 8.00 g of span 80, 0.27 g of azobisisobutyronitrile (AIBN), and 15.00 g of dodecane with stirring at room temperature. An aqueous discontinuous phase was prepared by adding 0.78 g potassium persulfate to 94.3 mL of distilled water. The oil phase was stirred at approximately 1400 rpm, and then the aqueous discontinuous phase was added to the oil phase at a flow rate of 20 mL/min. The combined phases were stirred at 1400 rpm for approximately 5−10 min to form a stable HIPE. An aqueous suspension medium was prepared by combining 2 g of potassium persulfate and 30 g of gelatin with 1 L of distilled water. The mixture was stirred at 250 rpm. The HIPE was added to the aqueous suspension medium in a 2 L reactor. To form particles, the suspension was polymerized by raising the temperature to 60 °C overnight (approximately 18 h) while stirring at 250 rpm. The resultant particles were washed 5 times with water, extracted with acetone using a Soxhlet extractor, and air-dried.

Alumina ALD on Porous Particles. A fluidized bed reactor was used to deposit alumina films on highly porous PS−DVB particles. This system has been described previously in detail.[33] A

(15) Mathieu, L. M.; Bourban, P. E.; Manson, J. A. E. Processing of homogeneous ceramic/polymer blends for bioresorbable composites. *Compos. Sci. Technol.* **2006**, *66* (11−12), 1606−1614.
(16) Nable, J.; Gulbinska, M.; Suib, S. L.; Galasso, F. Aluminum oxide coating on nickel substrate by metal organic chemical vapor deposition. *Surf. Coat. Technol.* **2003**, *173* (1), 74−80.
(17) Richards, V. N.; Vohs, J. K.; Fahlman, B. D.; Williams, G. L. Low temperature chemical vapor deposition of aluminosilicate thin films on carbon fibers. *J. Am. Ceram. Soc.* **2005**, *88* (7), 1973−1976.
(18) Nishino, J.; Nosaka, Y. Preparation of ZnO by a nearby vaporizing chemical vapor deposition method. *J. Mater. Res.* **2003**, *18* (9), 2029−2032.
(19) Suntola, T. Atomic layer epitaxy. *Thin Solid Films* **1992**, *216* (1), 84−89.
(20) George, S. M.; Ott, A. W.; Klaus, J. W. Surface chemistry for atomic layer growth. *J. Phys. Chem.* **1996**, *100* (31), 13121−13131.
(21) Dillon, A. C.; Ott, A. W.; Way, J. D.; George, S. M. Surface chemistry of Al_2O_3 deposition using $Al(CH_3)_3$ and H_2O in a binary reaction sequence. *Surf. Sci.* **1995**, *322* (1−3), 230−242.
(22) Ott, A. W.; Klaus, J. W.; Johnson, J. M.; George, S. M. Al_2O_3 thin film growth on Si(100) using binary reaction sequence chemistry. *Thin Solid Films* **1997**, *292* (1−2), 135−144.
(23) Wank, J. R.; George, S. M.; Weimer, A. W. Coating fine nickel particles with Al_2O_3 utilizing an atomic layer deposition-fluidized bed reactor (ALD-FBR). *J. Am. Ceram. Soc.* **2004**, *87* (4), 762−765.
(24) Wank, J. R.; George, S. M.; Weimer, A. W. Nanocoating individual cohesive boron nitride particles in a fluidized bed by ALD. *Powder Technol.* **2004**, *142* (1), 59−69.
(25) Hakim, L. F.; Blackson, J.; George, S. M.; Weimer, A. W. Nanocoating individual silica nanoparticles by atomic layer deposition in a fluidized bed reactor. *Chem. Vap. Deposition* **2005**, *11* (10), 420−425.
(26) Hakim, L. F.; George, S. M.; Weimer, A. W. Conformal nanocoating of zirconia nanoparticles by atomic layer deposition in a fluidized bed reactor. *Nanotechnology* **2005**, *16* (7), 375−381.
(27) Hakim, L. F.; McCormick, J. A.; Zhan, G. D.; Weimer, A. W.; Li, P.; George, S. M. Surface modification of titania nanoparticles using ultrathin ceramic films. *J. Am. Ceram. Soc.* **2006**, *89* (10), 3070−3075.
(28) Ferguson, J. D.; Weimer, A. W.; George, S. M. Atomic layer deposition of Al_2O_3 films on polyethylene particles. *Chem. Mater.* **2004**, *16* (26), 5602−5609.
(29) Wilson, C. A.; Grubbs, R. K.; George, S. M. Nucleation and growth during Al_2O_3 atomic layer deposition on polymers. *Chem. Mater.* **2005**, *17* (23), 5625−5634.
(30) Hakim, L. F.; Vaughn, C. L.; Dunsheath, H. J.; Carney, C. S.; Liang, X. H.; Li, P.; Weimer, A. W. Synthesis of oxidation-resistant metal nanoparticles via atomic layer deposition. *Nanotechnology* **2007**, *18* (34), art. No. 345603.
(31) Li, N. H.; Benson, J. R.; Kitagawa, N. Polymeric Microbeads and Method of Preparation. U.S. Patent 5,583,162, 1996.
(32) Li, N. H.; Benson, J. R.; Kitagawa, N. Polymeric Microbeads and Methods of Preparation. U.S. Patent 6,100,306, 2000.

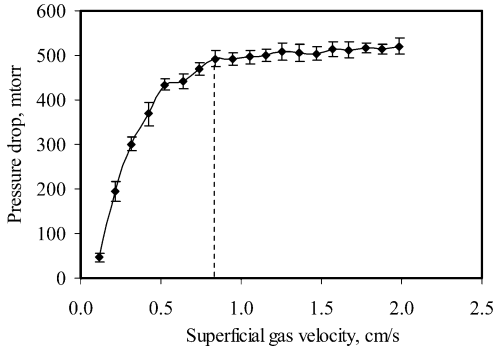

Figure 1. Pressure drop across the fluidized bed vs superficial gas velocity for porous polymer particles at 33 °C and reduced pressure.

fluidized bed reactor has the main advantages of excellent gas/particle contact and thermal efficiency and easy control due to stable operating conditions. For a typical run, about 4 g of porous particles was loaded into the reactor. The minimum pressure inside the reactor was about 50 mTorr, and the minimum fluidization superficial gas velocity was determined by measuring the pressure drop across the bed versus the N_2 superficial gas velocity. To obtain a baseline pressure profile, the pressure drop values were obtained without powder in the reactor. These values were then subtracted from the pressure drop values obtained for the reactor with powder. This provides the pressure drop resulting from the powder bed alone, as shown in Figure 1. Precursors, trimethylaluminum (TMA) obtained from Sigma Aldrich and deionized H_2O, were fed separately through the distributor of the reactor using the driving force of their vapor pressures. The flow rates of TMA and H_2O were adjusted using needle valves to ensure that the precursor pressure (∼3 Torr) was high enough for particle fluidization. A constant pressure of the precursor vapors was maintained during all the reactions.

Although the polymer substrate was highly porous, the reactor system was kept at high vacuum (∼50 mTorr) before TMA and H_2O exposures. The vapors (∼3 Torr) of TMA and H_2O can quickly diffuse into the pores of the particles and quickly complete the reaction. Therefore, the inside diffusion effect of the precursors can be neglected. The reaction temperature was 33 °C, which is much lower than the softening/melting point of the porous polymer particles. Before the reaction, the particles were outgassed at room temperature for 24 h. During each coating cycle, the precursors were fed for enough time so that saturation of all active sites occurred for every dose. A typical coating cycle used the following sequence: dose TMA, purge N_2, evacuate; dose H_2O, purge N_2, evacuate. In this manner, there was no overlap between the two reactants, and no undesirable CVD reactions occurred.

Analysis. The specific surface area of the PS−DVB particles was obtained using a Quantachrome Autosorb-1. The composition of the alumina films was confirmed using a PHI 5600 physical electronics X-ray photoelectron spectroscope with a high-energy resolution analyzer. The cross-sectional surface of the porous particles was observed with a JEOL JSM-7401F field emission scanning electron microscope equipped with an EDAXS detector unit for elemental analysis while imaging. The alumina films on the particle surface were visualized with energy dispersive spectroscopy (EDS) mapping. *Z*-contrast imaging of the coated samples was performed using a JEOL 2010F 200 kV Schottky field emission transmission electron microscope operating in the scanning trans-

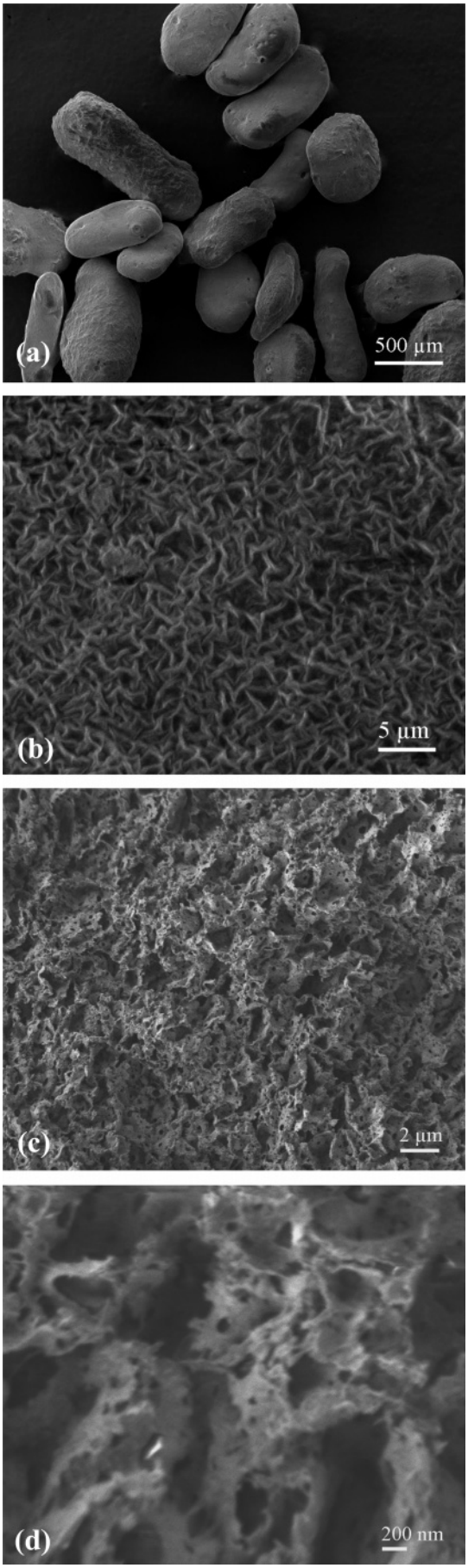

Figure 2. FESEM images of porous PS−DVB particles: (a) particles at low magnification, (b) particle surface at high magnification, and (c and d) cross-sectional surface at high magnification.

(33) Liang, X. H.; Hakim, L. F.; Zhan, G. D.; McCormick, J. A.; George, S. M.; Weimer, A. W.; Spencer, J. A.; Buechler, K. J.; Blackson, J.; Wood, C. J.; Dorgan, J. R. Novel processing to produce polymer/ceramic nanocomposites by atomic layer deposition. *J. Am. Ceram. Soc.* **2007**, *90* (1), 57−63.

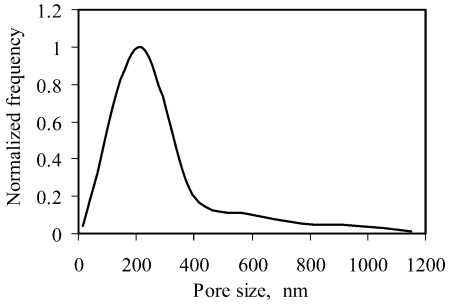

Figure 3. Size distribution of pores in porous polymer particles.

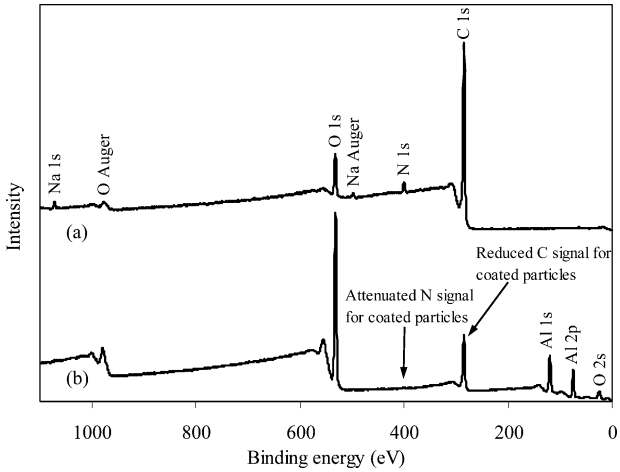

Figure 4. XPS spectra of (a) uncoated and (b) Al_2O_3 coated porous polymer particles after 50 cycles.

mission electron microscopy (STEM) mode with an electron probe size of 0.2 nm. Inductively coupled plasma atomic emission spectroscopy (ICP-AES) was performed using an Applied Research Laboratories ICP-AES 3410+.

Results and Discussion

Porous PS−DVB Particle Characterization. The average size of the synthesized PS−DVB particles was 600 μm. The highly porous structure of the particles was observed by field emission scanning electron microscopy (FESEM), as shown in Figure 2. On the basis of the FESEM images, the size distribution of the pores in the porous polymer particles is shown in Figure 3. The porosity of the porous particles was ∼85%, and the pore volume was in the range of 8−10 cm^3/g. The surface area of the particles was 43.5 ± 1.2 m^2/g, and the freely settled bulk density of the particles was 70 kg/m^3.

Test for Composition and Conformality of ALD Films. XPS measurements were obtained for uncoated and alumina coated porous PS−DVB particles after 50 ALD cycles. The analysis was performed using an aluminum source, pass energy of 187.85 eV, and energy step of 0.8 eV. In Figure 4, the spectrum for the uncoated porous polymer particles shows a strong C 1s photoelectron peak at 284.7 eV and weak N 1s, O 1s, and Na 1s peaks at 400, 530.7, and 1070 eV, respectively, which indicates that there are trace amounts of trapped solvent from the polymer synthesis process. In contrast, the carbon spectrum for coated particles reveals a much weaker photoelectron intensity at 284.7 eV, and the peaks of Na and N have been completely attenuated. This reduction of the C, N, and Na signals is expected if the

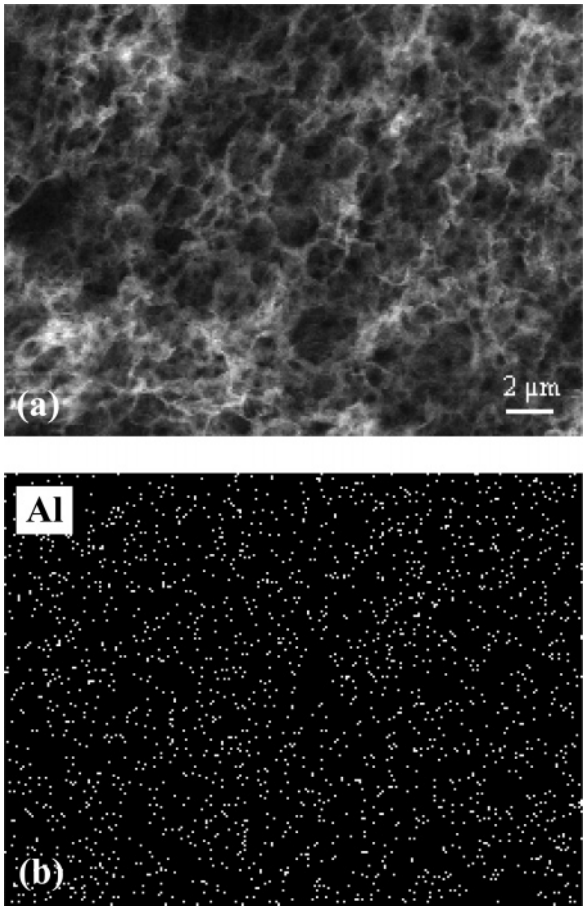

Figure 5. FESEM and EDS images of Al_2O_3 coated porous polymer particle: (a) FESEM image of cross-sectional surface of Al_2O_3 coated porous polymer particle after 25 cycles and (b) aluminum EDS signal of the same cross-sectional surface.

alumina films conformally cover the entire porous polymer particle surface. However, the carbon XPS signal cannot be completely attenuated as some of the carbon signal corresponds to surface carbon. Photoelectrons from the alumina coated particles are observed at 118.7 eV (Al, 2s), 73.9 eV (Al, 2p), and 530.7 eV (O, 1s). There is only a single peak centered at 73.9 eV, which corresponds to the Al−O bonds of alumina. The absence of a shoulder region around 72.5 eV, which corresponds to Al−Al bonds, clearly confirms that the aluminum metal is not present in the ALD films.[34,35] Thus, the XPS results verify the composition of deposited alumina on the porous polymer particles.

As long as the pores in the polymer substrate are larger than the ALD precursor molecules, the gases will diffuse into the pores and then deposit a uniform film. To ensure the deposition of alumina inside the pore structure and the distribution of alumina, the morphology of the coated porous particles was characterized by FESEM and EDS measurements. FESEM specimens were prepared by cutting the coated particles using a Super Gillette blue blade. As shown

(34) Jung, Y. C.; Miura, H.; Ohtani, K.; Ishida, M. High-quality silicon/insulator heteroepitaxial structures formed by molecular beam epitaxy using Al_2O_3 and Si. *J. Cryst. Growth* **1999**, *196* (1), 88−96.
(35) Yang, W. S.; Kim, Y. K.; Yang, S. Y.; Choi, J. H.; Park, H. S.; Lee, S. I.; Yoo, J. B. Effect of SiO_2 intermediate layer on $Al_2O_3/SiO_2/n(+)$-poly Si interface deposited using atomic layer deposition (ALD) for deep submicron device applications. *Surf. Coat. Technol.* **2000**, *131* (1−3), 79−83.

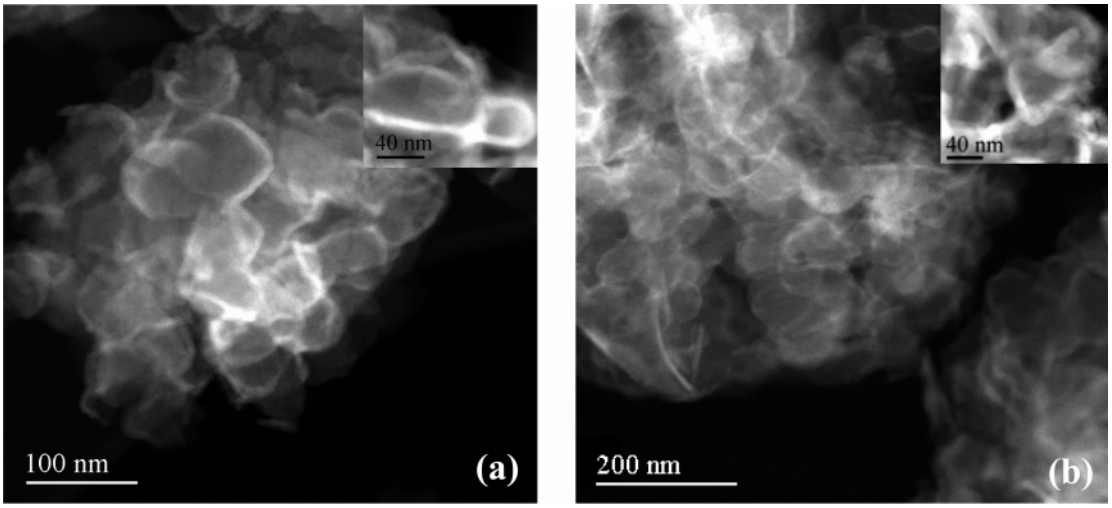

Figure 6. *Z*-contrast images of crushed Al_2O_3 coated porous polymer particles (a) after 25 cycles and (b) after 50 cycles.

in Figure 5, an aluminum EDS mapping signal illustrates the presence of alumina throughout the inner surface of the porous particles. Alumina films were formed inside the pores of the porous polymer and distributed homogeneously on the polymer surface.

The alumina coated porous polymer particles were analyzed by atomic resolution, *Z*-contrast imaging. Because of the difference in the atomic weight of the alumina and polymer, *Z*-contrast imaging is ideal in this case for analyzing the deposition of alumina films on polymer surfaces. TEM samples were prepared by placing the crushed porous particles on holey-carbon films supported on Cu grids. Representative *Z*-contrast images of the alumina coated polymer particles after 25 and 50 coating cycles are shown in Figure 6. The regions with a brighter contrast (i.e., regions with heavier *Z*) in Figure 6a,b were determined to be mostly alumina films by elemental nanoanalysis using EDS. The alumina films appear to be very uniform and smooth. The thickness of the alumina films is about 8 ± 2 and 15 ± 2 nm for coated particles after 25 cycles and 50 cycles, respectively, which represents a growth rate of about 0.3 nm per coating cycle at this experimental condition.

Cross-sectional TEM imaging allows precise observation at the edge interface of the polymer and alumina films. Cross-sectional TEM samples were prepared by cutting an epoxy resin cured porous polymer at a temperature of −100 °C using a diamond knife. The cross-sectional TEM image of porous PS−DVB particles after 25 cycles is shown in Figure 7. The black threads in the image are alumina films, which appear to be very uniform and smooth. Obviously, on the wall of some pores, there are no alumina films, which may have been peeled off during the cutting process. On the basis of the TEM image, approximately 7 ± 2 nm thick alumina films were coated on the wall of the pores of the polymer particle. This thickness also represents a growth rate of about 0.3 nm per coating cycle at this experimental condition, which corroborates the film thickness observed by STEM.

The alumina film growth rate is much higher than the 0.11 to 0.13 nm per cycle of an ALD process reported in the literature.[22] Recent FTIR measurements of alumina ALD on low-density polyethylene (LDPE) indicated the presence of

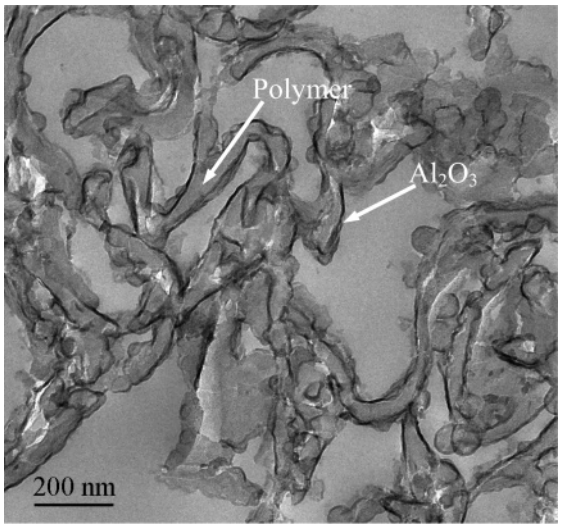

Figure 7. Cross-sectional TEM image of Al_2O_3 coated porous polymer particles after 25 cycles.

hydrogen bonded H_2O molecules on the alumina surface.[28] This higher growth rate may be explained by the presence of hydrogen bonded H_2O. This H_2O can react with TMA to deposit additional alumina by CVD.[28] Another reason is the increase in the surface coverage of reactants at lower temperatures.[36,37] Although the reaction kinetics is slower at lower temperatures, the growth rate is determined by the higher surface coverage.[36,37] Also, the growth rate of films may vary with the morphology of the substrate. For the highly porous polymer particles processed here having a surface area of 43.5 m^2/g, more active sites on the surfaces were exposed to the gas phase reactants. The different initial surfaces may be partly explained by the discrepancy between alumina growth rates on the porous PS−DVB particles and on some other substrates.

Pore Filling Mechanism. On the basis of STEM and cross-sectional TEM images, the alumina films were very

(36) Klaus, J. W.; Sneh, O.; George, S. M. Growth of SiO_2 at room temperature with the use of catalyzed sequential half-reactions. *Science (Washington, DC, U.S.)* **1997**, *278* (5345), 1934−1936.
(37) Groner, M. D.; Fabreguette, F. H.; Elam, J. W.; George, S. M. Low-temperature Al_2O_3 atomic layer deposition. *Chem. Mater.* **2004**, *16* (4), 639−645.

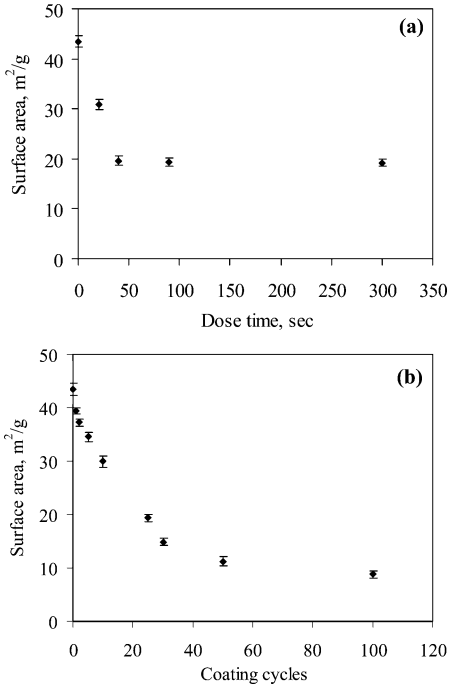

Figure 8. Surface area of porous polymer particles vs (a) precursor dose time (25 coating cycles) and (b) number of coating cycles (60 s dose time).

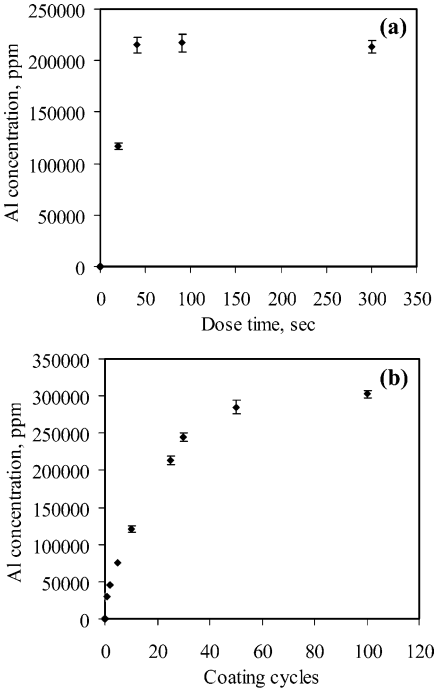

Figure 9. Aluminum concentration on porous polymer particles vs (a) precursor dose time (25 coating cycles) and (b) number of coating cycles (60 s dose time).

uniform and smooth, which may indicate that a pore filling mechanism of a conformal alumina growth process results. However, there is a variety of other pore filling mechanisms, including a gradual filling of the pores analogous to filling a pipe with water and a covering of the pore entrances.[38] To verify that the primary pore filling mechanism is a conformal coating of the pore walls under ALD growth, but not another filling mechanism, two series of experiments were carried out by varying the dose time of the precursors and the number of coating cycles. In the first series of experiments, the vapor pressures of the precursors, TMA and H_2O, were kept the same, the samples were exposed to 25 coating cycles, and the dose time of the precursors varied. In the second series of experiments, the vapor pressures of the precursors, TMA and H_2O, were also kept the same, and the dose time was 60 s, but the samples were exposed to different coating cycles. The surface area of the porous polymer/alumina composite material was analyzed by N_2 adsorption isotherms, and the concentration of aluminum on the porous polymer particles was analyzed by ICP-AES.

The surface area of the porous material is mainly from the internal surface area, and if the pores are filled with other materials, the internal surface area will decrease drastically. Hence, the specific surface area of the porous polymer will decrease if alumina films are coated within the pores. N_2 adsorption is a powerful method for the determination of the total surface area of the materials. The surface area of the BET measurements is shown in Figure 8. Figure 8a shows that the surface area of the samples decreases as a function of dose time, as the dose time decreases to some minimum value (40 s here). When the dose time is longer than this minimum (more than 40 s here), there is no additional surface area decrease, which verifies that the alumina ALD on the polymer is self-limiting and −terminating. Figure 8b shows the surface area of the samples versus the coating cycles. The surface area decreases greatly from 43.5 to 39.4 m^2/g after the first coating cycle and then decreases linearly as a function of coating cycles before 30 cycles, indicating a constant growth rate per AB cycle and a conformal alumina growth process. The surface area reduction is due to the pore volume reduction as the pore size decreases with increasing alumina films deposited on the pore walls. Once the nanoscale pores are filled with alumina, the surface area decreases less sharply. For example, from 50 cycles to 100 cycles, the reduction of surface area was only about 2.5 m^2/g, indicating that some nanoscale pores were inaccessible.

ICP-AES provides the concentration in parts per million (ppm) by the mass of aluminum in relation to the porous particles. Analysis by ICP-AES was performed by placing the coated porous PS−DVB particles in a strong base solution (NaOH) for at least 24 h to dissolve the alumina films from the porous polymer substrate. The ICP-AES aluminum concentration versus precursor dose time and number of coating cycles are shown in Figure 9. As shown in Figure 9a, for dose times less than some minimum value (40 s here), the amount of aluminum detected increases with dose time. When the dose time is 40 s or longer, there is no additional aluminum signal increment, which has the same trend of surface area versus dose time. This result also indicates that the alumina ALD reaction on the polymer is self-limiting and -terminating. Figure 9b shows that the concentration of aluminum is almost directly proportional to the number of coating cycles when the number of coating cycles is less than 30. This indicates a constant growth rate for the alumina film and a linear dependence between film

(38) Mahurin, S.; Bao, L. L.; Yan, W. F.; Liang, C. D.; Dai, S. Atomic layer deposition of TiO_2 on mesoporous silica. *J. Non-Cryst. Solids* **2006**, *352* (30−31), 3280−3284.

thickness and number of growth cycles. After 30 cycles, the increasing rate of increase of the aluminum concentration is much slower, which corroborates the result of surface area versus coating cycles. Obviously, there is no nucleation period. Porous PS−DVB particles have carbon−carbon double bonds, but they do not have hydroxyl groups to initiate the alumina ALD. Therefore, the initiation of alumina growth may result from the reaction between TMA and atmospheric exposure of water in the porous structure.

From the previously mentioned two sets of experiments, the pore filling mechanism of alumina ALD on this porous polymer is a conformal coating of the pore walls, since alumina ALD is self-limiting and -terminating, and the growth rate of alumina is a constant per AB cycle. On the basis of the BET surface area results, after 50 coating cycles, some nanoscale pores in the polymer were not accessible. Since the alumina ALD growth rate was about 0.3 nm per coating cycle, the nanoscale pores with sizes larger than 30 nm would be maintained after 50 cycles. For this kind of porous polymer, if the number of coating cycles was less than 30, the ultrathin alumina films provided for modifying the surface properties of porous polymer while keeping its porous structure property unchanged.

Conclusion

A process to synthesize a novel porous polymer/ceramic composite material was demonstrated. HIPE-based highly porous PS−DVB particles were synthesized by copolymerization of styrene and divinylbenzene. The synthesized PS−DVB particles have a porosity of ∼85%, a pore volume of 8−10 cm^3/g, a surface area of 43.5 m^2/g, and a density of 70 kg/m^3. Porous PS−DVB particles were successfully coated with alumina films at the atomic level in a fluidized bed reactor using a low-temperature scalable particle ALD process. The XPS measurements revealed that alumina films were deposited on the polymer particle surfaces. The results of EDS indicated that the alumina films were deposited throughout the inner and outer surfaces of the porous particles. STEM and cross-sectional TEM investigations revealed highly conformal and uniform alumina coatings. Combined with STEM and cross-sectional TEM, the surface area and aluminum concentration based on ICP-AES versus the precursor dose time and coating cycles revealed that the pore filling mechanism of alumina ALD for this highly porous polymer was a conformal coating of the pore walls. The ultrathin alumina films are expected to increase the biocompatibility of the polymer. This novel polymer/ceramic composite material with reinforced porous structures and enhanced bioactivity may have potential applications in tissue engineering. This novel surface treatment strategy provides a convenient and universal method for modifying the surface properties of porous polymer materials and thus a method to promote cell adhesion and proliferation for tissue engineering.

Acknowledgment. This work was partly supported by the National Science Foundation under Grant 0400292 and the Department of Energy under STTR Grant DE-FG02-03ER86157. Any opinions, findings, and conclusions or recommendations expressed in this work are those of the authors and do not necessarily reflect the views of the National Science Foundation or the Department of Energy. The authors thank Jarod A. McCormick at the University of Colorado for XPS analysis. The authors also thank Fred Luiszer at the University of Colorado for providing the ICP-AES analysis as well as Paul Rice at the University of Colorado for assistance with FESEM work.

CM071431K